Equivalent Impedance Electroelastic Modeling of Multiple Piezo-Patch Energy Harvesters on a Thin Plate With AC–DC Conversion

Amirreza Aghakhani, *Student Member, IEEE*, and Ipek Basdogan

***Abstract*—Piezo-patch energy harvesters can be readily attached to plate-like structures in automotive, marine, and aerospace applications, in order to exploit the broadband vibration of the host system. Power output investigations of such patch-based harvesters, when connected to practical interface circuits, require accurate models for harvesting performance evaluation and optimization. This paper proposes an analytical approach to derive the closed-form mechanical and electrical response expressions of the multiple piezo-patch energy harvesters (MPEHs) by integrating an equivalent load impedance, which consists of the harvesting circuit and the overall piezo-patch capacitance into a distributed-parameter model of the plate. Moreover, an equivalent circuit model of the electromechanical system is developed in a circuit simulator software SPICE for system-level simulations, taking into account the interconnection of piezo-patches and multiple vibration modes of the plate. Numerical SPICE simulations are then validated for the conventional ac input–ac output problem by the experiments and existing analytical solution. The proposed analytical model is validated by the experiments for the standard ac input–dc output problem. Finally, the analytical and numerical results for the peak power output of the MPEHs in series/parallel configuration with ac and dc interface circuits are presented, and shown to be in good agreement with the experimental results.**

***Index Terms*—Energy harvesting, equivalent impedance, Kirchhoff's plate, piezoelectricity, vibrations.**

I. Introduction

VIBRATION-BASED energy harvesting has received a great attention over the past decade with the ultimate goal of powering small electronic components, replacing the conventional batteries and thereby enabling self-powered systems [1]. Various vibration-to-electricity conversion methods have been used by researchers such as the electrostatic [2], electromagnetic [3], magnetostrictive [4], and piezoelectric transducers [5], as well as the dielectric elastomers [6]. Among these energy conversion approaches, piezoelectric transduction is the most favored one due to the high power density of piezoelectric materials and ease of implementation at different geometric scales [7], [8].

In the last two decades of piezoelectric energy harvesting literature, cantilever beam harvesters have been broadly investigated [9]–[13]. Major drawbacks of the typical cantilever beam harvesters are that power generation quickly drops when the excitation frequency is slightly different than the resonance frequency of the harvester especially in the low-damped harvesters, and also relatively large space between the first natural frequencies of cantilever beams limits the broadband energy harvesting. These downsides decrease the harvester efficiency in practical applications, where ambient vibrations are of varying frequency and random nature [14].

Piezoelectric patches can be readily integrated into thin plate-like structures, as an alternative to beam harvesters, to extract the vibrational energy of their host structure and convert it into electrical energy. The vast availability of thin plates-based structures in aerospace, automotive and marine applications, makes this implementation convenient to employ and provides broadband energy harvesting. In addition, piezo-patch energy harvesters attached to a thin plate have the merits of removing extra mass loading and volumetric occupancy as well as exhibiting a relatively large number of vibrational modes in a specific frequency range over the conventional cantilever designs. Few studies in the literature have focused on energy harvesting from two-dimensional (2-D) plate-like structures [15]–[17]. In the majority of modeling of both cantilever beam and plate-like harvesters, a resistance load is used to predict the ac power output. However, in practice, to transfer the electrically harvested power to the practical end devices (e.g., batteries and storage capacitor), a standard rectifier circuit is required to provide a stable dc output. In addition, a dc–dc converter can be used right after the rectifier to increase the power transfer performance [18]. Another technique called synchronized switch harvesting on inductor can be also utilized to maximize the extracted power [5]. Predicting the dynamic electromechanical response of the harvester(s) connected to practical circuits require high-fidelity analytical and/or numerical models. Liang and Liao [19], and Lien and Shu [20] have proposed equivalent load impedance method to obtain the steady-state electrical response of the harvester system connected to nonlinear circuits. The first group analyzed the system impedance using the fun-

Manuscript received October 25, 2016; revised February 2, 2017 and April 18, 2017; accepted June 3, 2017. Date of publication June 6, 2017; date of current version August 14, 2017. Recommended by Technical Editor D. Naso. This work was supported in part by the Scientific and Technical Research Council of Turkey (TUBITAK). *(Corresponding author: Ipek Basdogan.)*

The authors are with the Department of Mechanical Engineering, Koc University, Istanbul 34450, Turkey (e-mail: aaghakhani@ku.edu.tr; ibasdogan@ku.edu).

Color versions of one or more of the figures in this paper are available online at http://ieeexplore.ieee.org.

Digital Object Identifier 10.1109/TMECH.2017.2712713

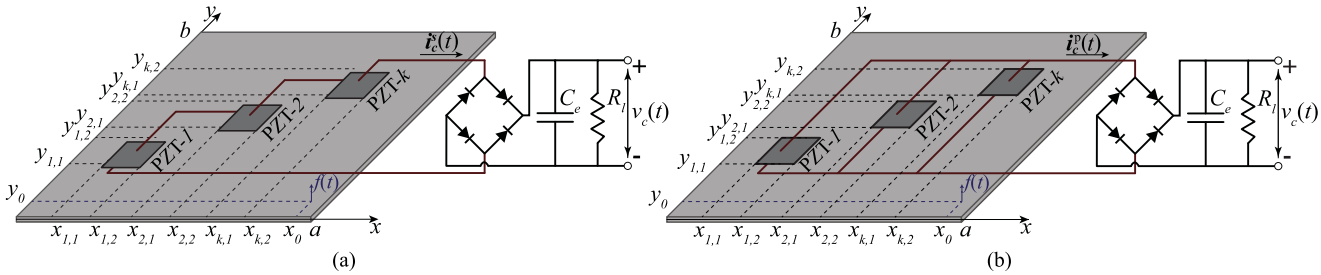

Fig. 1. Schematics of MPEHs attached to a thin plate and connected to an ac-dc converter with two connection configurations: (a) series; and (b) parallel. MPEHs: multiple piezo-patch energy harvesters.

damental Fourier mode of the harvesting circuit [19], whereas, the second group considered the principles of charge and energy balance [20]. Although these studies emphasized on the effect of different harvesting circuits on dynamics of the mechanical part, they modeled the host structure (i.e., cantilever beam) as a single-degree-of-freedom (SDOF) system that was similarly used in [18], [21], and [22]. This type of modeling neglects the distributed-parameters in continuous systems (e.g., beams and plates) along with other deficiencies that are reported in [23].

On the other hand, the mechanical part of the harvester system can be represented by an equivalent circuit model (ECM), where the system parameters can be obtained by an analogy between the second-order circuit and the electromechanically coupled equations. Then, the ECM of the harvester system can be developed in circuit simulation software (e.g., SPICE) for system-level simulations. Analytical [24] and numerical [25] methods were proposed for finding the equivalent circuit parameters of conventional base-excited beam harvesters. Recently, Bayik *et al*. [26] have presented the multimodal analytical and numerical methods for identifying the system parameters of a piezo-patch energy harvester attached to a thin plate.

Despite the efforts on the SDOF modeling of harvesters with nonlinear circuit interfaces, studies involving analytical closed-form solutions of 2-D structures (e.g., thin plates) with single/multiple piezo-patch harvesters connected to ac–dc circuits are not reported in the literature. The authors previously [27] showed that when the multiple piezo-patch harvesters are connected in parallel to a standard rectifier circuit, it is possible to obtain an analytical closed-form solution for the electrical response of the system. The analytical results of the dc voltage output for the first four vibration modes of the host plate were presented and validated by the numerical SPICE simulations, using the ECM of the multiple patch harvesting system in a parallel configuration (similar to the single patch case [26]). This paper presents an equivalent impedance electroelastic modeling of multiple piezo-patch energy harvesters (MPEHs) integrated into a thin plate and connected in series/parallel to a standard ac–dc converter circuit. The proposed analytical approach integrates the equivalent load impedance of the harvester into the distributed-parameter solution of the plate, thus, provides closed-form expressions for both the vibration and electrical responses of MPEHs with a practical nonlinear circuit. In addition, a generalized equivalent circuit modeling of a plate with MPEHs is introduced to be compatible with any connection types (i.e., series, parallel, and mixed series-parallel) of the patch harvesters, which fully incorporates the interconnection of piezo-patches, multiple vibration modes of the plates, and two-way electromechanical coupling effect. Using the proposed analytical and ECM models, electrical power outputs of MPEHs with the series and parallel configurations for a wide range of resistive loads in ac–ac and ac–dc cases are calculated. Experimental validations are also presented and shown to be in good agreement with the developed models.

II. Distributed-Parameter Model

In this section, a brief description of the distributed-parameter model of a thin plate with MPEHs is given based on Kirchhoff plate theory. Fig. 1 presents the host plate with all four edges clamped (CCCC) boundary conditions and the structurally integrated piezoelectric patches in series and parallel configurations connected to a standard ac–dc converter circuit. The host plate with the length and width of a and b is excited by a transverse point force $f(t)$ acting at the position coordinates (x_0, y_0). The plate thickness $(h_{\bar{\mathrm{s}}})$ is assumed to be much smaller than other dimensions so that the effects of transverse shear deformation are neglected based on the Kirchhoff plate theory. Hereafter, the subscripts $\bar{\mathrm{s}}$ and $\bar{\mathrm{p}}$ stand for the parameters related to the host structure and piezoelectric patch, respectively. The total number of piezo-patch harvesters is $n_{\bar{\mathrm{p}}}$ and the thickness of kth patch is $(h_{\bar{\mathrm{p}}})_k$. In the electromechanical equations of the thin plate, mass and stiffness contribution of piezoelectric patches have been neglected due to the small volume ratio of the patch to the host plate and only induced moments of piezoelectric patches at the electrode boundaries are included. However, it has been shown for a nondeterministic thin plate that the mass effect of the piezo-patch becomes important at high frequencies [28].

The following sections express the electromechanical equations of MPEHs that were previously developed by Aridogan *et al*. [29] for the case of the simplified electrical circuit, namely a resistive load.

A. Electromechanical Equations for Series Configuration

The electrical circuit representation of series configurations of MPEHs with ac–dc conversion is shown in Fig. 2. Each piezo-patch harvester is represented by a velocity proportional current source in parallel to an equivalent piezoelectric capacitance.

The coupled circuit equation for each piezo-patch harvester can be expressed as

$$(C_{\bar{\mathrm{p}}})_k \frac{\mathrm{d}v_k^{\mathrm{s}}(t)}{\mathrm{d}\,t} + i_c^{\mathrm{s}}(t) = i_k^{\mathrm{s}}(t) \tag{1}$$

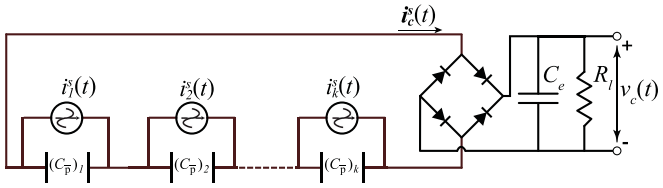

Fig. 2. Electrical circuit representation for series configuration of MPEHs connected to a standard ac–dc converter. Each piezo-patch harvester is equivalently composed of a velocity proportional current generator and a piezo capacitance connected in parallel.

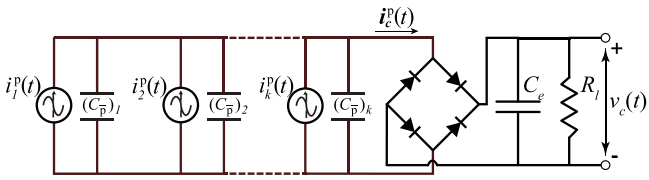

Fig. 3. Electrical circuit representation for parallel configuration of MPEHs connected to a standard ac–dc converter. Each piezo-patch harvester is equivalently composed of a velocity proportional current generator and a piezo capacitance connected in parallel.

where $k = 1, 2, ..., n_{\bar{p}}$, $v_k^s(t)$, and $i_k^s(t)$ are the voltage across the electrodes and current source of the kth piezo-patch harvester, whereas, the current flowing through the interface circuit is denoted by $i_c^s(t)$. The equivalent piezoelectric capacitance can be written as [29]

$$(C_{\bar{p}})_k = (\bar{\varepsilon}_{33}^S)_k \frac{(l_{\bar{p}})_k (w_{\bar{p}})_k}{(h_{\bar{p}})_k} \tag{2}$$

where the piezo-patch dimension terms $(l_{\bar{p}})_k$, $(w_{\bar{p}})_k$, and $(h_{\bar{p}})_k$ are the length, width, and thickness of the kth patch harvester, respectively, and $(\bar{\varepsilon}_{33}^S)_k$ is the permittivity of the kth piezo-patch at constant strain.

The electromechanically coupled mechanical and electrical equations in modal coordinates can be presented as [29]

$$\frac{d^2\eta_{mn}^s(t)}{dt^2} + 2\zeta_{mn}\omega_{mn}\frac{d\eta_{mn}^s(t)}{dt} + \omega_{mn}^2\eta_{mn}^s(t) - \sum_{k=1}^{n_{\bar{p}}}(\tilde{\theta}_{mn})_k v_k^s(t) = f_{mn}(t) \tag{3}$$

$$\sum_{n=1}^{\infty}\sum_{m=1}^{\infty}(\tilde{\theta}_{mn})_k \frac{d\eta_{mn}^s(t)}{dt} + (C_{\bar{p}})_k \frac{dv_k^s(t)}{dt} + i_c^s(t) = 0 \tag{4}$$

where ω_{mn} and ζ_{mn} are the corresponding undamped natural frequency and modal damping ratio for the mnth vibration mode. From the electrical equations in (1) and (4), the velocity dependent current source of the kth harvester for the series configuration can be obtained as

$$i_k^s(t) = -\sum_{n=1}^{\infty}\sum_{m=1}^{\infty}(\tilde{\theta}_{mn})_k \frac{d\eta_{mn}^s(t)}{dt} \tag{5}$$

where $\eta_{mn}^s(t)$ is the modal coordinate of the plate for the mnth vibration mode and the electromechanical coupling term $(\tilde{\theta}_{mn})_k$ is given by [29]

$$(\tilde{\theta}_{mn})_k = \theta_k \int_{y_{k,1}}^{y_{k,2}}\int_{x_{k,1}}^{x_{k,2}} \left[\frac{\partial^2\varphi_{mn}(x,y)}{\partial x^2} + \frac{\partial^2\varphi_{mn}(x,y)}{\partial y^2}\right] dxdy \tag{6}$$

where $\varphi_{mn}(x,y)$ is the mass-normalized eigenfunction of the plate for the mnth vibration mode at (x,y) location. The electromechanical term θ_k is defined as $\theta_k = (h_{pc})_k(\bar{e}_{31})_k$, where $(\bar{e}_{31})_k$ is the effective piezoelectric constant, and $(h_{pc})_k$ is the reference distance of the center layer of kth piezo-patch from the neutral surface of the plate. Moreover, the modal forcing input in (3) is given by [29]

$$f_{mn}(t) = f(t)\varphi_{mn}(x_0, y_0) \tag{7}$$

B. Electromechanical Equations for Parallel Configuration

The electrical circuit representation of the parallel configuration of MPEHs is shown in Fig. 3.

The governing equation of the coupled circuit dynamics can be written as

$$\frac{dv^p(t)}{dt}\sum_{k=1}^{n_{\bar{p}}}(C_{\bar{p}})_k + i_c^p(t) = i^p(t) \tag{8}$$

where $i^p(t)$ is a summation of the all current sources, that is $i^p(t) = \sum_{k=1}^{n_{\bar{p}}} i_k^p(t)$, and $(C_{\bar{p}})_k$ is the equivalent piezoelectric capacitance defined in (2). The voltage across each piezo-patch electrodes is equal, which means $v^p = v_k^p(t)$, and the current flowing through the interface circuit is denoted by $i_c^p(t)$.

The electromechanically coupled modal equations can be presented for the parallel configuration of the MPEHs as [29]

$$\frac{d^2\eta_{mn}^p(t)}{dt^2} + 2\zeta_{mn}\omega_{mn}\frac{d\eta_{mn}^p(t)}{dt} + \omega_{mn}^2\eta_{mn}^p(t) - v^p(t)\sum_{k=1}^{n_{\bar{p}}}(\tilde{\theta}_{mn})_k = f_{mn}(t) \tag{9}$$

$$\sum_{k=1}^{n_{\bar{p}}}\sum_{n=1}^{\infty}\sum_{m=1}^{\infty}(\tilde{\theta}_{mn})_k \frac{d\eta_{mn}^p(t)}{dt} + \frac{dv^p(t)}{dt}\sum_{k=1}^{n_{\bar{p}}}(C_{\bar{p}})_k + i_c^p(t) = 0. \tag{10}$$

Consequently, from (8) and (10) the velocity proportional current source of kth harvester can be expressed as

$$i_k^p(t) = -\sum_{n=1}^{\infty}\sum_{m=1}^{\infty}(\tilde{\theta}_{mn})_k \frac{d\eta_{mn}^p(t)}{dt} \tag{11}$$

where $\eta_{mn}^p(t)$ is the modal coordinate of the plate for the mnth vibration mode.

III. Equivalent Impedance Modeling

Solving the electromechanical equations given in Sections II-A and II-B under steady-state conditions for the series/parallel configurations of MPEHs connected to a single resistance would be straightforward [29]. However, for the practical harvesting circuits which consist of nonlinear elements such as diodes, another approach is required to derive the exact solution. To this end, the Sections III-A and III-B propose the idea of using equivalent load impedance to develop

the closed-form expressions for the mechanical and electrical responses of MPEHs. Moreover, Section III-C details the equivalent circuit modeling of the mechanical part for the case of multiple harvesters.

A. Equivalent Impedance of the Electrical Domain for the Series Configuration

For the ac–dc converter circuit shown in Fig. 2, the current flowing into the ideal rectifier circuit $i_c^{\mathrm{s}}(t)$ can be defined as the piecewise equation

$$i_c^{\mathrm{s}}(t) = \begin{cases} C_e \dot{v}_c^{\mathrm{s}}(t) + \frac{v_c^{\mathrm{s}}(t)}{R_l} & \text{if } v^{\mathrm{s}} = v_c^{\mathrm{s}} \\ -C_e \dot{v}_c^{\mathrm{s}}(t) - \frac{v_c^{\mathrm{s}}(t)}{R_l} & \text{if } v^{\mathrm{s}} = -v_c^{\mathrm{s}} \\ 0 & \text{if } |v^{\mathrm{s}}| < v_c^{\mathrm{s}} \end{cases} \tag{12}$$

where $v^s(t)$ is the overall piezoelectric voltage defined as $v^{\mathrm{s}}(t) = \sum_{k=1}^{n_{\bar{\mathrm{p}}}} v_k^{\mathrm{s}}(t)$, and $v_c^s(t)$ is the dc voltage across the resistive load for the series configuration. If the smoothing capacitor is carefully chosen so that the time constant $R_l C_e$ is much larger than the period of the excitation, the dc voltage output would have a constant V_c^{s} magnitude, and the ripple in the rectified voltage would be negligible for large values of smoothing capacitor [5], [30].

The current balance equation in (4) can be rearranged to be in the form

$$\frac{\mathrm{d}v_k^{\mathrm{s}}(t)}{\mathrm{d}\,t} + \frac{i_c^{\mathrm{s}}(t)}{(C_{\bar{\mathrm{p}}})_k} = \frac{-\sum_{n=1}^{\infty}\sum_{m=1}^{\infty}(\tilde{\theta}_{mn})_k \frac{\mathrm{d}\eta_{mn}^{\mathrm{s}}(t)}{\mathrm{d}t}}{(C_{\bar{\mathrm{p}}})_k}. \tag{13}$$

Let the equivalent voltage source for the kth piezo-patch harvester be defined as

$$\hat{v}_k(t) = \sum_{m=1}^{\infty}\sum_{n=1}^{\infty}(\hat{v}_{mn}(t))_k\,,\ (\hat{v}_{mn}(t))_k = -\frac{(\tilde{\theta}_{mn})_k \eta_{mn}^{\mathrm{s}}(t)}{(C_{\bar{\mathrm{p}}})_k} \tag{14}$$

which taking the summation of both sides in (13) over k from 1 to $n_{\bar{\mathrm{p}}}$ and using (14) gives

$$\frac{\mathrm{d}v^{\mathrm{s}}(t)}{\mathrm{d}\,t} + \frac{i_c^{\mathrm{s}}(t)}{C_{\bar{\mathrm{p}}}^{\mathrm{eq,s}}} = \frac{\mathrm{d}\hat{v}(t)}{\mathrm{d}\,t} \tag{15}$$

where $\hat{v}(t) = \sum_{k=1}^{n_{\bar{\mathrm{p}}}} \hat{v}_k(t)$ is referred to the overall equivalent voltage source and $C_{\bar{\mathrm{p}}}^{\mathrm{eq,s}} = (\sum_{k=1}^{n_{\bar{\mathrm{p}}}} (C_{\bar{\mathrm{p}}})_k^{-1})^{-1}$.

Now, based on linear system assumption, if the transverse point force applied on the surface of the plate is of the form $f(t) = F_0 e^{j\omega t}$, the steady-state responses of modal coordinate of the plate, the kth piezoelectric capacitance voltage, and the kth equivalent voltage source can be written as

$$\eta_{mn}^{\mathrm{s}}(t) = \mathrm{H}_{mn}^{\mathrm{s}} e^{j\omega t} \tag{16}$$

$$v_k^{\mathrm{s}}(t) = \mathrm{V}_k^{\mathrm{s}} e^{j\omega t} \tag{17}$$

$$\hat{v}_k(t) = -\sum_{m=1}^{\infty}\sum_{n=1}^{\infty}\frac{(\tilde{\theta}_{mn})_k \mathrm{H}_{mn}^{\mathrm{s}} e^{j\omega t}}{(C_{\bar{\mathrm{p}}})_k} = \hat{\mathrm{V}}_k e^{j\omega t} \tag{18}$$

where $\mathrm{H}_{mn}^{\mathrm{s}}$, $\mathrm{V}_k^{\mathrm{s}}$, and $\hat{\mathrm{V}}_k$ are the complex amplitudes. Further, the steady-state form of the overall equivalent voltage source can be expressed as $\hat{v}(t) = \hat{\mathrm{V}} e^{j\omega t}$ with $\hat{\mathrm{V}} = \sum_{k=1}^{n_{\bar{\mathrm{p}}}} \hat{\mathrm{V}}_k$.

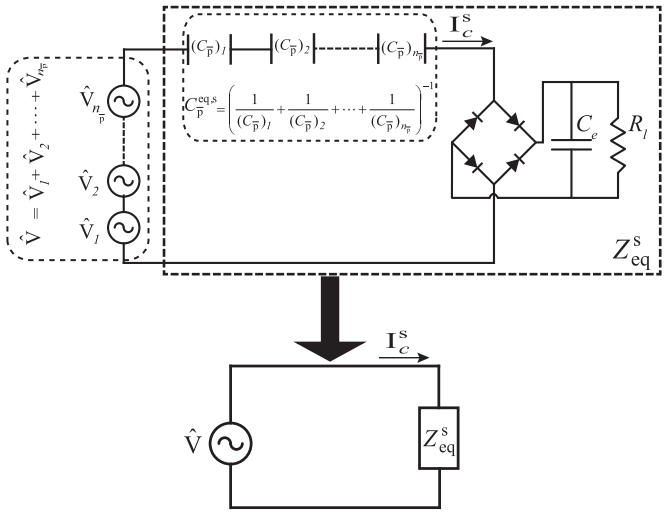

Fig. 4. Top diagram shows array of piezo-patch harvesters connected in series to a standard ac–dc circuit, where each harvester is represented by an equivalent voltage source connected to a piezo capacitance in series. In the bottom diagram, the overall capacitance plus the ac–dc circuit is replaced by an equivalent impedance $Z_{\mathrm{eq}}^{\mathrm{s}}$ connected to the overall voltage source.

Having substituted the steady-state forms of the $\eta_{mn}^{\mathrm{s}}(t)$ and $v_k^{\mathrm{s}}(t)$ into (3) and (4), the complex model response $\mathrm{H}_{mn}^{\mathrm{s}}$ can be obtained by extracting the $\mathrm{V}_k^{\mathrm{s}}$ from (4) and substituting into (3)

$$\mathrm{H}_{mn}^{\mathrm{s}} = \frac{F_0 \varphi_{mn}(x_0, y_0) + \sum_k^{n_{\bar{\mathrm{p}}}} (\tilde{\theta}_{mn})_k \mathrm{V}_k^{\mathrm{s}}}{{\omega_{mn}}^2 - \omega^2 + j2\zeta_{mn}\omega_{mn}\omega}. \tag{19}$$

Integrating the (15) over the half-cycle period of the excitation (e.g., time interval in which $\hat{v}(t)$ goes from minimum $-\hat{\mathrm{V}}$ to maximum $\hat{\mathrm{V}}$), while using the piecewise equation in (12) yields

$$V_c^s = \frac{C_{\bar{\mathrm{p}}}^{\mathrm{eq,s}} \omega R_l}{\pi/2 + C_{\bar{\mathrm{p}}}^{\mathrm{eq,s}} \omega R_l} \hat{\mathrm{V}}. \tag{20}$$

The next step is to find the complex equivalent voltage $\hat{\mathrm{V}}_k$ and the complex voltage $\mathrm{V}_k^{\mathrm{s}}$ for $k = 1, 2, \ldots, n_{\bar{\mathrm{p}}}$, so that the dc voltage output can be obtained readily from (20), and the complex modal amplitude $\mathrm{H}_{mn}^{\mathrm{s}}$ can be obtained from (19).

Fig. 4 shows the electrical circuit representation of (15) for the MPEHs in a series configuration. This electrical representation unlike the one shown in Fig. 2, can facilitate the analytical modeling. In addition, the harvesting circuit (i.e., ac–dc converter) plus the overall capacitance of piezo-patches can be represented as an equivalent load impedance $Z_{\mathrm{eq}}^{\mathrm{s}}$. Suppose that the $Z_{\mathrm{eq}}^{\mathrm{s}}$ is known for the range of excitation frequencies, then the current going through it (Kirchhoff's circuit law) is

$$\mathrm{I}_c^{\mathrm{s}} = \frac{1}{Z_{\mathrm{eq}}^{\mathrm{s}}}\hat{\mathrm{V}} = \frac{1}{Z_{\mathrm{eq}}^{\mathrm{s}}}\sum_{k=1}^{n_{\bar{\mathrm{p}}}} \hat{\mathrm{V}}_{\mathrm{k}} \tag{21}$$

where $\mathrm{I}_c^{\mathrm{s}}$ is the complex amplitude of the current $i_c^{\mathrm{s}}(t)$. Here, to determine the $Z_{\mathrm{eq}}^{\mathrm{s}}$, we use the model proposed by Lin *et al.* [31], who obtained the equivalent load impedance for the array of SDOF harvesters connected in series to the ac–dc converter circuit and showed that the equivalent impedance is the function

of excitation frequency, equivalent piezoelectric capacitance, and resistive load. Therefore, it is independent of the number of vibrational modes and can be safely adopted for our case.

The complex impedance model is defined as $Z^{\mathrm{s}}_{\mathrm{eq}} = (Z^{\mathrm{s}}_R - jZ^{\mathrm{s}}_I)^{-1}$, where the real and imaginary parts are given by [31]

$$Z^s_R = \frac{2(C^{\mathrm{eq,s}}_{\bar{\mathrm{p}}})^2\omega^2 R_l}{(\pi/2 + C^{\mathrm{eq,s}}_{\bar{\mathrm{p}}}\omega R_l)},\ Z^s_I = \frac{-\pi C^{\mathrm{eq,s}}_{\bar{\mathrm{p}}}\omega}{2(\pi/2 + C^{\mathrm{eq,s}}_{\bar{\mathrm{p}}}\omega R_l)}. \quad (22)$$

Now, taking a time derivative of (3), replacing $\frac{d}{dt}(v^{\mathrm{s}}_k(t))$ with that of (13), and finally substituting the steady-state forms from (16), (18), and (21), the modal mechanical equation reduces to

$$\begin{aligned}&\left(\omega^2_{mn} - \omega^2 + j2\zeta_{mn}\omega_{mn}\omega\right)\cdot \mathrm{H}^s_{mn}\\ &+\sum_{k=1}^{n_{\bar{\mathrm{p}}}}\left[\frac{1}{j\omega Z^s_{\mathrm{eq}}}\cdot\sum_{k=1}^{n_{\bar{\mathrm{p}}}}\left(\frac{(\tilde{\theta}_{mn})_k}{(C_{\bar{\mathrm{p}}})_k}\right) - (\tilde{\theta}_{mn})_k\right]\cdot\hat{\mathrm{V}}_k\\ &\quad = F_0\phi_{mn}(x_0,\ y_0).\end{aligned} \quad (23)$$

Then, multiplying both sides in (24) by $(\tilde{\theta}_{mn})_k/(C_{\bar{\mathrm{p}}})_k \cdot (\omega^2_{mn} - \omega^2 + j2\zeta_{mn}\omega_{mn}\omega)^{-1}$, and taking double summation over *m* by *n* number of vibrational modes, the resulting equation can be rewritten in a matrix equation of the form

$$(\mathbf{Q} - \mathbf{I})\hat{\mathbf{V}} = \hat{\mathbf{F}} \quad (24)$$

where $\hat{\mathbf{V}}$ is $n_{\bar{\mathrm{p}}} \times 1$ unknown vector and equals to $\hat{\mathbf{V}} = [\hat{\mathrm{V}}_1\ \hat{\mathrm{V}}_2\ \cdots\ \hat{\mathrm{V}}_{n_{\bar{\mathrm{p}}}}]^T$, $\mathbf{I}$ is the identity matrice with the dimensions of $n_{\bar{\mathrm{p}}} \times n_{\bar{\mathrm{p}}}$. Besides, $\mathbf{Q}$ as a square matrix with the dimensions of $n_{\bar{\mathrm{p}}} \times n_{\bar{\mathrm{p}}}$, and $\hat{\mathbf{F}}$ as a column vector with the dimensions of $n_{\bar{\mathrm{p}}} \times 1$ are given by

$$Q_{ij} = \sum_{m=1}^{\infty}\sum_{n=1}^{\infty}\left[\frac{(\tilde{\theta}_{mn})_i}{(C_{\bar{\mathrm{p}}})_i}\times\frac{\frac{1}{j\omega Z^s_{\mathrm{eq}}}\sum_{k=1}^{n_{\bar{\mathrm{p}}}}\frac{(\tilde{\theta}_{mn})_k}{(C_{\bar{\mathrm{p}}})_k} - (\tilde{\theta}_{mn})_j}{(\omega^2_{mn} - \omega^2 + j2\zeta_{mn}\omega_{mn}\omega)}\right] \quad (25)$$

$$\hat{f}_i = F_0\cdot\sum_{m=1}^{\infty}\sum_{n=1}^{\infty}\left[\frac{(\tilde{\theta}_{mn})_i}{(C_{\bar{\mathrm{p}}})_i}\times\frac{\varphi_{mn}(x_0,y_0)}{(\omega^2_{mn} - \omega^2 + j2\zeta_{mn}\omega_{mn}\omega)}\right]. \quad (26)$$

Having solved for each $\hat{\mathrm{V}}_k$ in (24), the steady-state magnitude of dc voltage across the resistive load can be obtained from (20).

The complex equivalent voltage $\hat{\mathrm{V}}_k$ can be substituted into (15), considering (17) and (18), to obtain the complex voltage $\mathrm{V}^{\mathrm{s}}_k$ as

$$\mathrm{V}^{\mathrm{s}}_k = \hat{\mathrm{V}}_k - \frac{1}{j\omega(C_{\bar{\mathrm{p}}})_k Z^{\mathrm{s}}_{\mathrm{eq}}}\sum_{k=1}^{n_{\bar{\mathrm{p}}}}\hat{\mathrm{V}}_k. \quad (27)$$

The resulting complex voltage $\mathrm{V}^{\mathrm{s}}_k$ can be substituted into (19) to obtain the complex $\mathrm{H}^{\mathrm{s}}_{mn}$. Next, the transverse displacement response of the plate at point (*x*,*y*), and time *t* can be obtained, based on the modal analysis procedure, by substituting $\eta^{\mathrm{s}}_{mn}(t)$ into the following:

$$\begin{aligned}w^{\mathrm{s}}(x,y,t) &= \sum_{m=1}^{\infty}\sum_{n=1}^{\infty}\varphi_{mn}(x,y)\cdot\eta^{\mathrm{s}}_{mn}(t)\\ &= \sum_{m=1}^{\infty}\sum_{n=1}^{\infty}\left\{\frac{\varphi_{mn}(x,y)}{{\omega_{mn}}^2 - \omega^2 + j2\zeta_{mn}\omega_{mn}\omega}\right.\\ &\quad\cdot\left(F_0\varphi_{mn}(x_0,y_0) + \sum_{k=1}^{n_{\bar{\mathrm{p}}}}(\tilde{\theta}_{mn})_k\hat{\mathrm{V}}_k\right.\\ &\quad\left.\left. - \frac{1}{j\omega Z^{\mathrm{s}}_{\mathrm{eq}}}\sum_{k=1}^{n_{\bar{\mathrm{p}}}}\frac{(\tilde{\theta}_{mn})_k}{(C_{\bar{\mathrm{p}}})_k}\cdot\sum_{k=1}^{n_{\bar{\mathrm{p}}}}\hat{\mathrm{V}}_{\mathrm{k}}\right)\right\}\cdot e^{j\omega t}.\end{aligned} \quad (28)$$

After formulating the steady-state vibration response, the electromechanical FRF can be extracted for the transverse displacement-to-force input ratio with $\beta^{\mathrm{s}}(w,x,y) = w^{\mathrm{s}}(x,y,t)/(F_0e^{jwt})$. The velocity FRF, velocity-to-force input ratio, can be directly derived from the displacement FRF as $\beta^{\mathrm{s,velocity}}(w,x,y) = j\omega\beta^{\mathrm{s}}(w,x,y)$. It should be noted that all the complex $\hat{\mathrm{V}}_{\mathrm{k}}$'s inherit the amplitude F_0 from (23), which eventually cancels out with the F_0 in the denominator of displacement FRF $\beta^{\mathrm{s}}(w,x,y)$.

B. Equivalent Impedance of the Electrical Domain for the Parallel Configuration

Likewise for the parallel configuration of MPEHs, the current flowing into the ac–dc converter circuit, $i^{\mathrm{p}}_c(t)$ shown in Fig. 3, is related to the rectified voltage $v^{\mathrm{p}}_c(t)$ by the piecewise equation similar to (12).

For the harmonic excitations at frequency ω, the applied force input is of the form $f(t) = F_0e^{j\omega t}$. The steady-state mechanical modal response $\eta^{\mathrm{p}}_{mn}(t)$, and the steady-state voltage response of piezo-patch harvesters $v^{\mathrm{p}}(t)$ based on the linear system assumption can be expressed as

$$\eta^{\mathrm{p}}_{mn}(t) = \mathrm{H}^{\mathrm{p}}_{mn}e^{j\omega t} \quad (29)$$

$$v^{\mathrm{p}}(t) = \mathrm{V}^{\mathrm{p}}e^{j\omega t} \quad (30)$$

where $\mathrm{H}^{\mathrm{p}}_{mn}$ and V^{p} are both complex valued. Next, by inserting the steady-state forms into (8) and (9), the complex modal response $\mathrm{H}^{\mathrm{p}}_{mn}$ can be obtained as

$$\mathrm{H}^{\mathrm{p}}_{mn} = \frac{F_0\varphi_{mn}(x_0,y_0) + \mathrm{V}^{\mathrm{p}}\sum_k^{n_{\bar{\mathrm{p}}}}(\tilde{\theta}_{mn})_k}{\omega^2_{mn} - \omega^2 + j2\zeta_{mn}\omega_{mn}\omega}. \quad (31)$$

The velocity dependent current source in (11) can be expressed with the steady-state form of $i^{\mathrm{p}}_k(t) = \mathrm{I}^{\mathrm{p}}_k e^{jwt}$ where the complex amplitude is

$$\mathrm{I}^{\mathrm{p}}_k = \sum_{n=1}^{\infty}\sum_{m=1}^{\infty}(\mathrm{I}^{\mathrm{p}}_{mn})_k = \sum_{n=1}^{\infty}\sum_{m=1}^{\infty}\left[-j\omega(\tilde{\theta}_{mn})_k\mathrm{H}^{\mathrm{p}}_{mn}\right] \quad (32)$$

and the overall velocity proportional current source can be written as the summation of all the dependent current source terms

$$i^{\mathrm{p}}(t) = \mathrm{I}^{\mathrm{p}}e^{j\omega t} = \sum_{k=1}^{n_{\bar{\mathrm{p}}}}\mathrm{I}^{\mathrm{p}}_k e^{j\omega t}. \quad (33)$$

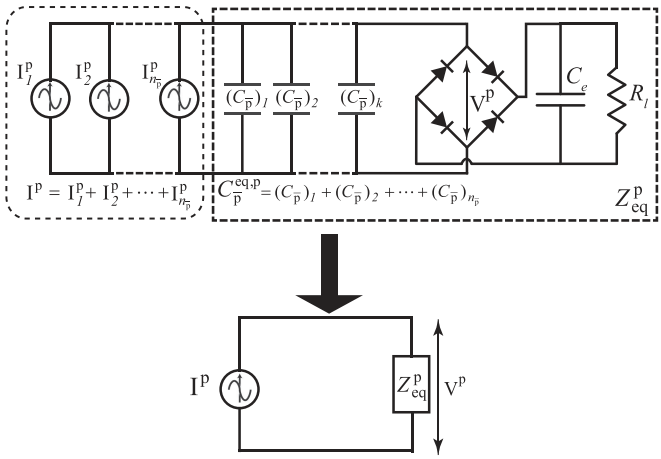

Fig. 5. Top diagram shows array of piezo-patch harvesters connected in parallel to a standard ac–dc circuit, where each harvester is represented by an equivalent current source connected to a piezo capacitance in parallel. In the bottom diagram, the overall capacitance plus the ac–dc circuit is replaced by an equivalent impedance Z_{eq}^p connected to the overall current source.

The average dc voltage output of the harvester, under the steady-state operation, can be obtained by integrating the current balance equation in (8) over the half-cycle period of the excitation as follows:

$$V_c = \frac{R_l}{\pi/2 + (R_l\omega)C_{\bar{p}}^{eq,p}} I^p. \tag{34}$$

Here, $C_{\bar{p}}^{eq,p}$ is the overall equivalent piezoelectric capacitance for the piezopatches in parallel, and expressed as $C_{\bar{p}}^{eq,p} = \sum_{k=1}^{n_{\bar{p}}} (C_{\bar{p}})_k$.

Now for determining the dc voltage in (35), all the I_k^p's for $k = 1, 2, ..., n_{\bar{p}}$ need to be found out. To do so, let Z_{eq}^p be the equivalent impedance for the parallel configuration which consists of the ac–dc circuit and the overall equivalent piezo capacitance as shown in Fig. 5. Lien and Shu [20] proposed the equivalent impedance model for the array of SDOF harvesters connected in parallel to an ac–dc converter which is adopted here as well. The reason of validity of this model was discussed in Section III-A. The complex equivalent impedance is defined as $Z_{eq}^p = Z_R^p + jZ_I^p$ where the real and imaginary parts are given by [20]

$$Z_R^p = \frac{2R_l}{(\pi/2 + C_{\bar{p}}^{eq,p} R_l\omega)^2}, \quad Z_I^p = -\frac{R_l}{(\pi/2 + C_{\bar{p}}^{eq,p} R_l\omega)}. \tag{35}$$

The complex magnitudes of equivalent current source and voltage across Z_{eq}^p in Fig. 5 are related by

$$V^p = Z_{eq}^p \cdot I^p = Z_{eq}^p \cdot \sum_{k=1}^{n_{\bar{p}}} I_k^p. \tag{36}$$

Substituting the steady-state forms of $v^p(t)$ and $\eta_{mn}^p(t)$ into (9), the mechanical equation for the parallel configuration of MPEHs reduces to

$$(\omega_{mn}^2 - \omega^2 + j2\zeta_{mn}\omega_{mn}\omega)H_{mn}^p - Z_{eq}^p \left(\sum_{k=1}^{n_{\bar{p}}} I_k^p\right) \sum_{k=1}^{n_{\bar{p}}} (\tilde{\theta}_{mn})_k = F_0\varphi_{mn}(x_0, y_0). \tag{37}$$

Then, dividing both sides of the above equation by $\sum_{k=1}^{n_{\bar{p}}} (\tilde{\theta}_{mn})_k$, and using (32), the resultant can be rearranged to be in the form of matrix equation as

$$\mathbf{Z}^* \mathbf{I}^* = \mathbf{V}^* \tag{38}$$

where $\mathbf{I}^*$ is the unknown column vector with the dimensions of $mn \times 1$ including the equivalent current amplitudes of each vibration mode as $\mathbf{I}^* = [\, I_{11}^p \; I_{21}^p \cdots I_{mn}^p \,]^T$. In addition, the known column vector $\mathbf{V}^*$ with the dimensions of $mn \times 1$ defined as $\mathbf{V}^* = [\, V_{11}^* \; V_{21}^* \cdots V_{mn}^* \,]^T$ and the square matrix $\mathbf{Z}^*$ with the dimensions of $mn \times mn$ are given by

$$V_{ij}^* = \frac{-F_0\varphi_{ij}(x_0, y_0)}{\sum_{k=1}^{n_{\bar{p}}} (\tilde{\theta}_{ij})_k}, \; i = 1, 2, \ldots, m, \; j = 1, 2, \ldots, n \tag{39}$$

$$\mathbf{Z}^* = \mathrm{diag}(\mathbf{Z}) + Z_{eq}^p \mathbf{J} \tag{40}$$

where $\mathbf{J}$ is an all-ones matrix with the dimensions of $mn \times mn$, and $\mathrm{diag}(\mathbf{Z})$ is a diagonal matrix, whose diagonal elements are the elements of the vector $\mathbf{Z}$ with the dimensions of $mn \times 1$ that is defined as $\mathbf{Z} = [\, Z_{11} \; Z_{21} \cdots Z_{mn} \,]^T$, where

$$Z_{rs} = \frac{2\zeta_{rs}\omega_{rs}}{\left(\sum_{k=1}^{n_{\bar{p}}} (\tilde{\theta}_{rs})_k\right)^2} + j\frac{\omega^2 - \omega_{rs}^2}{\omega\left(\sum_{k=1}^{n_{\bar{p}}} (\tilde{\theta}_{rs})_k\right)^2}$$
$$r = 1, 2, \ldots, m, \; s = 1, 2, \ldots, n. \tag{41}$$

Therefore, by solving the linear equations in (38) for the unknown vector $\mathbf{I}^*$, the steady-state magnitude of dc voltage across the resistive load can be obtained from (34).

The complex H_{mn}^p can be extracted from (37) to determine the mechanical modal coordinate $\eta_{mn}^p(t)$ which can be then substituted in the following equation to obtain the transverse displacement response of the plate at point (x,y), and time t:

$$w^p(x, y, t) = \sum_{m=1}^{\infty}\sum_{n=1}^{\infty} \varphi_{mn}(x, y) \cdot \eta_{mn}^p(t)$$
$$= \sum_{n=1}^{\infty}\sum_{m=1}^{\infty} \left\{ \frac{\varphi_{mn}(x, y)}{{\omega_{mn}}^2 - \omega^2 + j2\zeta_{mn}\omega_{mn}\omega} \cdot \left(F_0\varphi_{mn}(x_0, y_0) + Z_{eq}^p \cdot \sum_{m=1}^{\infty}\sum_{n=1}^{\infty} I_{mn}^p \cdot \sum_{k=1}^{n_{\bar{p}}} (\tilde{\theta}_{mn})_k \right) \right\} \cdot e^{j\omega t}. \tag{42}$$

The transverse displacement-to-force input FRF can be expressed as $\beta^p(w, x, y) = w^p(x, y, t)/(F_0 e^{jwt})$, and the velocity FRF can be obtained as $\beta^{p,\mathrm{velocity}}(w, x, y) = j\omega\beta^p(w, x, y)$. Again, notice that all the complex I_{mn}^p's include the force

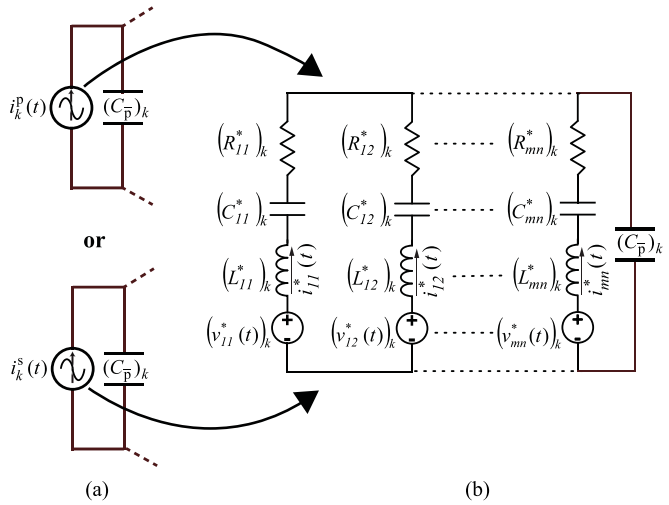

Fig. 6. This diagram illustrates the procedure for developing the multimode ECM of the MPEHs. Arrows indicate that the *k*th piezo-patch harvester branch in series or parallel configuration shown in (a), is represented by a set of $m \times n$ secondary-order circuits connected in parallel to a piezo capacitance (each subbranch represents a single vibration mode of the host system), as shown in (b). The ECM of the whole system can then be obtained by connecting a total of $n_{\bar{p}}$ branches in series or parallel configuration.

amplitude F_0 from (38), resulting in the cancellation of the term F_0 in the displacement FRF.

C. Equivalent Circuit Modeling

Representation of the mechanical part of piezoelectric energy harvesters, in a linear regime, by the equivalent circuit, is studied well in the literature. The studies presented an ECM for a piezoelectric layer on a beam [24], [25], [32], a piezo-patch on the plate [26], and an array of individual cantilever harvesters in series [31] and parallel configurations [20]. In all the aforementioned ECMs, each piezoelectric energy harvester is attached to a single host structure. However, in our case, multiple piezo-patch harvesters share a common host system to exploit the multiple vibration modes, thus, a certain ECM is required to take into account the interconnection of piezo-patches and their electromechanical coupling effect on the plate.

Fig. 6 demonstrates the equivalent circuit modeling for the *k*th piezo-patch harvester, where the dependent current source is represented by a set of secondary-order circuits. Having repeated this procedure for $k = 1, 2, \ldots, n_{\bar{p}}$, in parallel and series configurations (see Figs. 2 and 3), the full electromechanical behavior of the multiple piezo-patch harvesters while connected to a practical interface circuit, can be predicted via an electronic circuit simulator (e.g., SPICE).

According to the analogy between the analytical distributed-parameter expressions given in (3) and (9), and the ECM in Fig. 6, system parameters are obtained and summarized in Table I. It's worth pointing out the dissimilarities in the system parameters for single versus multiple piezo-patch harvesters integrated into a thin plate. In the single patch harvester case [26], for each vibration mode, there is just a single coupling term $\tilde{\theta}_{mn}$ in the elements of mechanical impedance with $R^*_{mn} = 2\zeta_{mn}\omega_{mn}/\tilde{\theta}^2_{mn}$, $L^*_{mn} = 1/\tilde{\theta}^2_{mn}$, $C^*_{mn} = \tilde{\theta}^2_{mn}/\omega^2_{mn}$, and the equivalent voltage source with $v^*_{mn}(t) = -f_{mn}(t)/\theta_{mn}$. However, in the case of multiple patch harvesters, these equivalent terms of the single harvester cannot be simply mapped into the *k*th piezo-patch harvester and regarded as an independent parameter, which is why the system parameters are different for the MPEHs.

TABLE I
ANALOGY BETWEEN ELECTRICAL AND MECHANICAL DOMAINS OF MPEHS

Equivalent circuit parameters	Mechanical counterparts
Electrical current: $(i^*_{mn}(t))_k$	$-(\tilde{\theta}_{mn})_k \dot{\eta}^{\mathrm{p}}_{mn}(t)$ or $-(\tilde{\theta}_{mn})_k \dot{\eta}^{\mathrm{s}}_{mn}(t)$
Voltage source: $(v^*_{mn}(t))_k$	$-f_{mn}(t)/\sum_{k=1}^{n_{\bar{p}}}(\tilde{\theta}_{mn})_k$
Inductance: $(L^*_{mn})_k$	$1/((\tilde{\theta}_{mn})_k \sum_{k=1}^{n_{\bar{p}}}(\tilde{\theta}_{mn})_k)$
Resistance: $(R^*_{mn})_k$	$2\zeta_{mn}\omega_{mn}/((\tilde{\theta}_{mn})_k \sum_{k=1}^{n_{\bar{p}}}(\tilde{\theta}_{mn})_k)$
Capacitance: $(C^*_{mn})_k$	$((\tilde{\theta}_{mn})_k \sum_{k=1}^{n_{\bar{p}}}(\tilde{\theta}_{mn})_k)/\omega^2_{mn}$

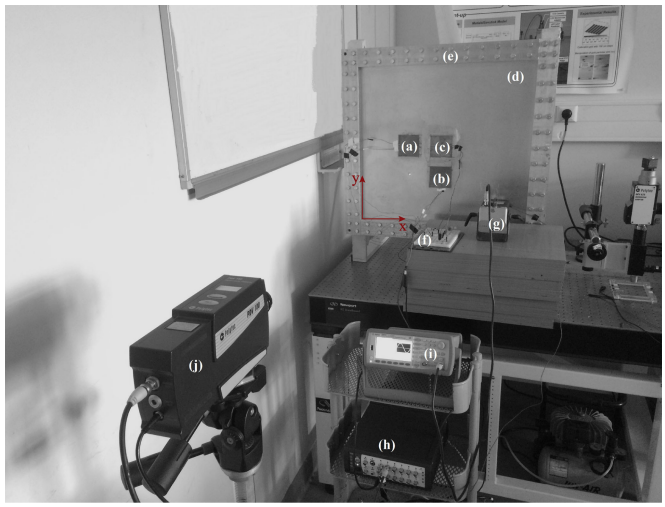

Fig. 7. Experimental setup: (a) PZT-1; (b) PZT-2; (c) PZT-3; (d) aluminum plate; (e) clamping frame; (f) electrical circuit; (g) modal shaker with a force transducer; (h) data acquisition unit; (i) signal generator; and (j) laser vibrometer

IV. Model Validations

A. Experimental Setup

Fig. 7 presents the experimental setup used for analyzing the harvesting performance of multiple piezo-patch configurations and validating the analytical and ECM models. The transversely isotropic piezoceramic patches (T105-A4E-602 manufactured by Piezo Systems, Inc.) are installed as piezo-patch energy harvesters on the aluminum plate. The dynamic point force loading is measured by a force transducer (PCB 208C02) attached to the plate at 0.085 and 0.085 m away from the bottom right corner of the plate. The velocity outputs are measured via a laser Doppler vibrometer (Polytec PDV 100). Two general experiment cases are examined in this study, namely ac input – ac output case and ac input – dc output case. In the first case, the

TABLE II
GEOMETRIC, MATERIAL, AND ELECTROELASTIC PROPERTIES

Property	Aluminum	Piezoceramic
Length (mm)	580	72.4
Width (mm)	540	72.4
Thickness (mm)	1.9	0.267
Young's modulus (GPa)	65.1	66
Mass density (kg/m^{-3})	2575	7800
Piezoelectric constant d_{31} (pm/V)	–	-190
Permittivity constant $\bar{\varepsilon}_{33}^{S}$ (nF/m)	–	10.38

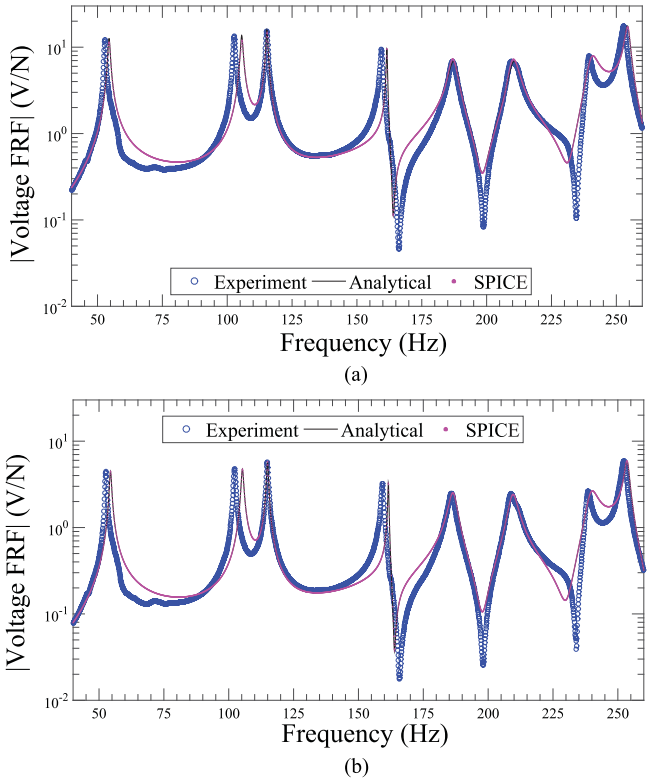

Fig. 8. AC input—ac output case: Comparison of experiment, analytical model, and SPICE simulations for voltage FRF of MPEHs in (a) series and (b) parallel configurations with open-circuit condition.

aluminum plate is excited by a linear sine sweep signal over the bandwidth of 20–260 Hz through a modal shaker. The voltage FRFs are directly measured from the two terminals of the resistive load. For the second experiment case, the sweep rate is selected as slow enough to ensure considerable charge time for the smoothing capacitor, and as fast enough to avoid lengthy experiment data. The rectifier circuit consists of four commercially available Schottky diodes (BAT85), which are known for their fast switching performance and the low voltage drop (typically around 0.2 V [33]), and a smoothing capacitor followed by a resistive load. For both case studies, the geometric, material, and electroelastic properties are given in Table II.

B. AC Input–AC Output Case

Fig. 8 presents the steady-state voltage FRFs of the MPEHs with series and parallel configurations under the effect of

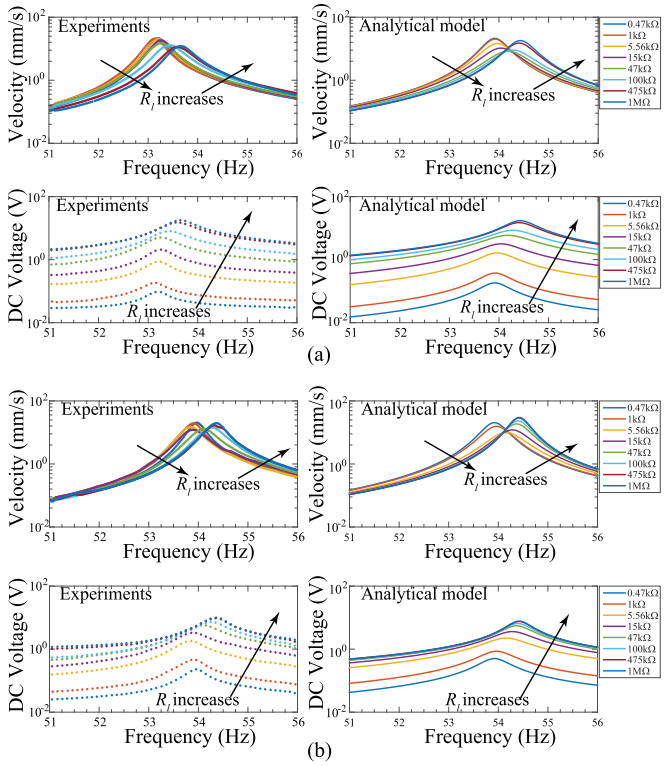

Fig. 9. Variations of the first mode velocity and dc voltage outputs of the harvester for the range of resistive loads subjected to 1 N point force excitation: (a) Series configuration; and (b) parallel configuration. Experiment data are shown in the left column and analytical results in the right column. Arrows indicate the direction of increase in resistive load value.

a harmonic point force, close to the open-circuit condition ($R_l = 1\,\mathrm{M}\Omega$). The ac–ac numerical simulation results, considering 5×5 vibration modes of the plate, accurately match with the existing analytical model presented by Aridogan *et al.* [29], and experiments. The modal damping ratios can be extracted from the experimental velocity or voltage FRFs with an arbitrary resistive load used in the harvesting circuit [1]. It can be observed from Fig. 8 that overall open-circuit voltage output magnitudes of series configuration are larger than the ones in the parallel configuration, which is in line with the series circuit assumption. Also in the fourth, fifth, sixth, and seventh vibration modes, peak voltages are significantly smaller than the other resonance frequencies, where the reason can be explained by the charge cancellation of the piezo-patches due to the strain distributions [29].

C. AC Input–DC Output Case

The analytical and experimental velocity and dc voltage outputs of the patch harvesters at the excitation frequencies around the first vibration mode for eight values of resistive loads in series and parallel configurations are shown in Fig. 9, respectively. The harmonic force excitation magnitude for the first vibration mode is around 1 N. Although the analytical model developed in this work ignores the real behavior of the diodes, it reasonably follows the trend of experimental velocity and voltage responses.

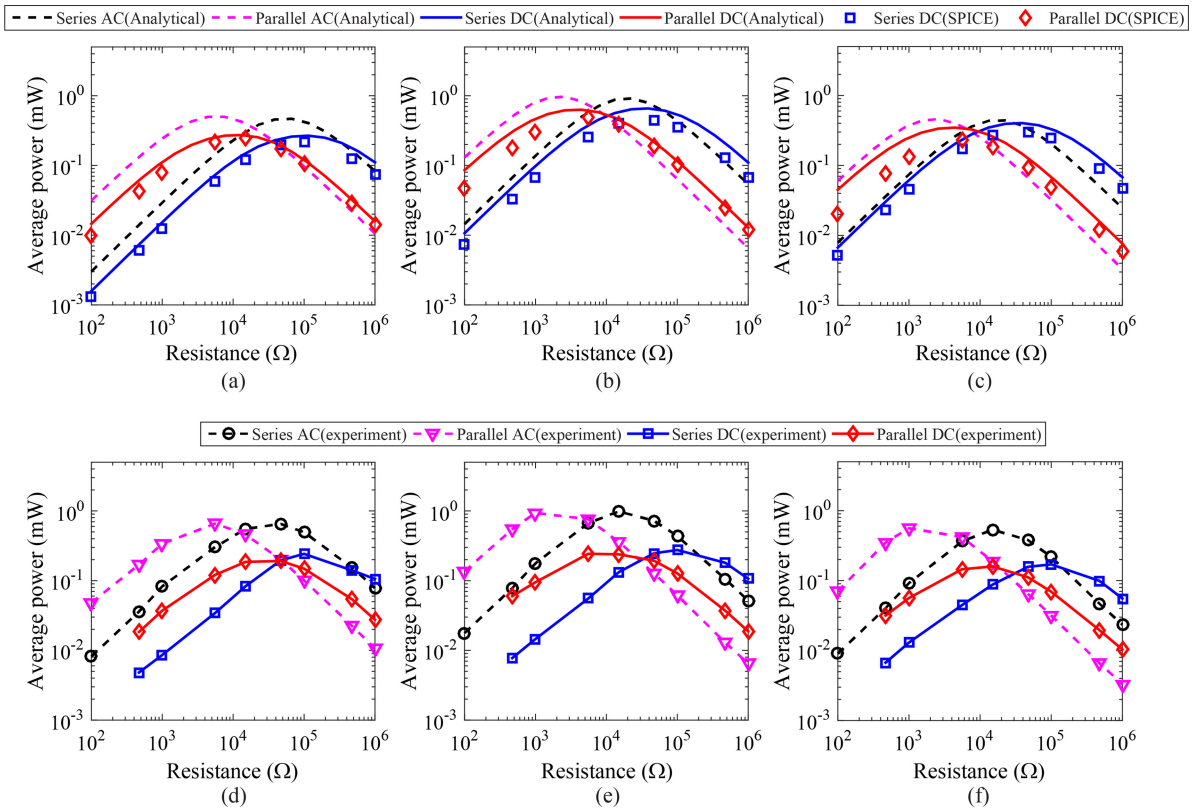

Fig. 10. Comparison of peak power outputs for the ac input–ac output and ac input–dc output cases versus load resistance. Analytical model and SPICE simulation: (a) First mode; (b) second mode; and (c) third mode. Experiment data: (d) First mode; (e) second mode; and (f) third mode.

Fig. 10 shows the analytical, numerical, and experimental results of average power output versus load resistance for the first three vibration mode, where the peak amplitudes are extracted at the open-circuit resonance frequencies. The load resistance values used in the experiments are 100 Ω, 470 Ω, 1 kΩ, 5.56 kΩ, 15 kΩ, 47 kΩ, 100 kΩ, 475 kΩ, and 1 MΩ. Here, the magnitudes of sinusoidal external force for the first three vibration modes, in the open-circuit conditions, are measured by the force transducer as 0.72 N, 0.53 N, and 0.32 N, respectively. The graphs in the upper row exhibit the analytical predictions and SPICE simulations for the peak ac and dc voltage outputs of MPEHs for the first three vibration modes, whereas the graphs in the bottom row show the experimental data. The overall average power levels for each vibration mode in ac–dc case are lower than the corresponding ac–ac, which can be referred mainly to the electrical loss. The optimum resistive load value, where the average power is maximum, is larger for the series configuration than that for the parallel configuration in both ac–ac and ac–dc cases. Additionally, the optimal load resistance of both the series and parallel configuration in ac-dc is slightly shifted to a larger value, when compared to the ac–ac case. The SPICE simulations always underestimate the analytical model predictions, by taking into account voltage drop of the rectifier circuit, and tend to be closer to the experiment results. Overall, the analytical and SPICE predictions agree well with the experimental data for a wide range of resistive loads.

V. Conclusion

In this paper, an analytical and a numerical approach is proposed for modeling MPEHs attached to thin plates with practical circuit interface. The analytical model integrates the equivalent impedance of the harvesting circuit into the distributed-parameter electroelastic model of the plate with multiple patch harvesters. Analytical predictions for the steady-state velocity response and dc voltage output of the MPEHs in series and parallel configurations are presented for a wide range of resistive loads around the first resonance frequency and validated by the experimental results. The ECM of the electromechanical system is developed for any connection types of the harvesters and validated for the ac–ac case by the existing analytical solution and experiments. Moreover, peak power outputs of the harvester with standard ac–ac and ac-dc configurations are predicted for the first three vibration modes as a function of varying load resistance. The equivalent impedance electroelastic model and the ECM developed in this work, which can be extended to other distributed-parameter systems with integrated single/multiple piezo-patch harvesters, allow evaluating the performance of such systems for design improvement and power optimization.

References

[1] D. J. Inman, A. Erturk, and D. J. Inman, *Piezoelectric Energy Harvesting*. Hoboken, NJ, USA: Wiley, 2011.

[2] E. O. Torres and G. A. Rincón-Mora, "Electrostatic energy-harvesting and battery-charging CMOS system prototype," *IEEE Trans. Circuits Syst. I, Reg. Papers*, vol. 56, no. 9, pp. 1938–1948, Sep. 2009.
[3] P. Constantinou, P. H. Mellor, and P. D. Wilcox, "A magnetically sprung generator for energy harvesting applications," *IEEE/ASME Trans. Mechatronics*, vol. 17, no. 3, pp. 415–424, Jun. 2012.
[4] D. Davino, A. Giustiniani, C. Visone, and W. Zamboni, "Stress-induced eddy currents in magnetostrictive energy harvesting devices," *IEEE Trans. Magn.*, vol. 48, no. 1, pp. 18–25, Jan. 2012.
[5] D. Guyomar, A. Badel, E. Lefeuvre, and C. Richard, "Toward energy harvesting using active materials and conversion improvement by nonlinear processing," *IEEE Trans. Ultrason., Ferroelect., Freq. Control*, vol. 52, no. 4, pp. 584–594, Apr. 2005.
[6] S. J. A. Koh, C. Keplinger, T. Li, S. Bauer, and Z. Suo, "Dielectric elastomer generators: How much energy can be converted?," *IEEE/ASME Trans. Mechatronics*, vol. 16, no. 1, pp. 33–41, Feb. 2011.
[7] K. A. Cook-Chennault, N. Thambi, and A. M. Sastry, "Powering MEMS portable devices—A review of non-regenerative and regenerative power supply systems with special emphasis on piezoelectric energy harvesting systems," *Smart Mater. Struct.*, vol. 17, no. 4, Aug. 2008, Art. no. 43001.
[8] S. R. Anton and H. A. Sodano, "A review of power harvesting using piezoelectric materials (2003-2006)," *Smart Mater. Struct.*, vol. 16, no. 3, pp. R1–R21, Jun. 2007.
[9] F. Khameneifar, S. Arzanpour, and M. Moallem, "A piezoelectric energy harvester for rotary motion applications: Design and experiments," *IEEE/ASME Trans. Mechatronics*, vol. 18, no. 5, pp. 1527–1534, 2013.
[10] A. Erturk and D. J. Inman, "A distributed parameter electromechanical model for cantilevered piezoelectric energy harvesters," *J. Vib. Acoust.*, vol. 130, no. 4, 2008, Art. no. 41002.
[11] X. Zheng *et al.*, "Analysis of energy harvesting performance for d15 mode piezoelectric bimorph in series connection based on timoshenko beam model," *IEEE/ASME Trans. Mechatronics*, vol. 20, no. 2, pp. 728–739, Apr. 2015.
[12] M. F. Lumentut and I. M. Howard, "Electromechanical piezoelectric power harvester frequency response modeling using closed-form boundary value methods," *IEEE/ASME Trans. Mechatronics*, vol. 19, no. 1, pp. 32–44, Feb. 2014.
[13] M. F. Lumentut and I. M. Howard, "Effect of shunted piezoelectric control for tuning piezoelectric power harvesting system responses—analytical techniques," *Smart Mater. Struct.*, vol. 24, no. 10, Oct. 2015, Art. no. 105029.
[14] S. Roundy, P. K. Wright, and J. Rabaey, "A study of low level vibrations as a power source for wireless sensor nodes," *Comput. Commun.*, vol. 26, no. 11, pp. 1131–1144, Jul. 2003.
[15] C. De Marqui Junior, A. Erturk, and D. J. Inman, "An electromechanical finite element model for piezoelectric energy harvester plates," *J. Sound Vib.*, vol. 327, no. 1/2, pp. 9–25, 2009.
[16] S. Lee and B. D. Youn, "A new piezoelectric energy harvesting design concept: Multimodal energy harvesting skin," *IEEE Trans. Ultrason., Ferroelect. Freq. Control*, vol. 58, no. 3, pp. 629–645, Mar. 2011.
[17] U. Aridogan, I. Basdogan, and A. Erturk, "Analytical modeling and experimental validation of a structurally integrated piezoelectric energy harvester on a thin plate," *Smart Mater. Struct.*, vol. 23, no. 4, Apr. 2014, Art. no. 45039.
[18] G. K. Ottman, H. F. Hofmann, A. C. Bhatt, and G. A. Lesieutre, "Adaptive piezoelectric energy harvesting circuit for wireless remote power supply," *IEEE Trans. Power Electron.*, vol. 17, no. 5, pp. 669–676, Sep. 2002.
[19] J. Liang and W.-H. Liao, "Impedance modeling and analysis for piezoelectric energy harvesting systems," *IEEE/ASME Trans. Mechatronics*, vol. 17, no. 6, pp. 1145–1157, Dec. 2012.
[20] I. C. Lien and Y. C. Shu, "Array of piezoelectric energy harvesting by the equivalent impedance approach," *Smart Mater. Struct.*, vol. 21, no. 8, Aug. 2012, Art. no. 82001.
[21] A. M. Wickenheiser, T. Reissman, and E. Garcia, "Modeling the effects of electromechanical coupling on energy storage through piezoelectric energy harvesting," *IEEE/ASME Trans. Mechatronics*, vol. 15, no. 3, pp. 400–411, Jun. 2010.
[22] Y. C. Wu, E. Halvorsen, M. Lallart, C. Richard, and D. Guyomar, "Stochastic modeling in the frequency domain for energy harvester with switching electronic interface," *IEEE/ASME Trans. Mechatronics*, vol. 20, no. 1, pp. 59–60, Feb. 2015.
[23] A. Erturk and D. J. Inman, "Issues in mathematical modeling of piezoelectric energy harvesters," *Smart Mater. Struct.*, vol. 17, no. 6, p. 65016, Dec. 2008.
[24] N. G. Elvin and A. A. Elvin, "A general equivalent circuit model for piezoelectric generators," *J. Intell. Mater. Syst. Struct.*, vol. 20, no. 1, pp. 3–9, Jan. 2009.
[25] Y. Yang and L. Tang, "Equivalent circuit modeling of piezoelectric energy harvesters," *J. Intell. Mater. Syst. Struct.*, vol. 20, no. 18, pp. 2223–2235, Dec. 2009.
[26] B. Bayik, A. Aghakhani, I. Basdogan, and A. Erturk, "Equivalent circuit modeling of a piezo-patch energy harvester on a thin plate with AC–DC conversion," *Smart Mater. Struct.*, vol. 25, no. 5, May 2016, Art. no. 55015.
[27] A. Aghakhani, I. Basdogan, and A. Erturk, "Multiple piezo-patch energy harvesters integrated to a thin plate with AC-DC conversion: analytical modeling and numerical validation," *Proc. SPIE*, vol. 9806, 2016, Art. no. 98060C.
[28] A. G. A. Muthalif, A. N. Wahid, and K. A. M. Nor, "Estimating ensemble average power delivered by a piezoelectric patch actuator to a non-deterministic subsystem," *J. Sound Vib.*, vol. 333, no. 4, pp. 1149–1162, 2014.
[29] U. Aridogan, I. Basdogan, and A. Erturk, "Multiple patch-based broadband piezoelectric energy harvesting on plate-based structures," *J. Intell. Mater. Syst. Struct.*, vol. 25, no. 14, pp. 1664–1680, Sep. 2014.
[30] Y. C. Shu and I. C. Lien, "Analysis of power output for piezoelectric energy harvesting systems," *Smart Mater. Struct.*, vol. 15, no. 6, pp. 1499–1512, Dec. 2006.
[31] H. C. Lin, P. H. Wu, I. C. Lien, and Y. C. Shu, "Analysis of an array of piezoelectric energy harvesters connected in series," *Smart Mater. Struct.*, vol. 22, no. 9, p. 94026, Sep. 2013.
[32] L. Tang, L. Zhao, Y. Yang, and E. Lefeuvre, "Equivalent circuit representation and analysis of galloping-based wind energy harvesting," *IEEE/ASME Trans. Mechatronics*, vol. 20, no. 2, pp. 834–844, Apr. 2015.
[33] R. Tiwari, K. Ryoo, A. Schlichting, and E. Garcia, "Extremely low-loss rectification methodology for low-power vibration energy harvesters," *Smart Mater. Struct.*, vol. 22, no. 6, Jun. 2013, Art. no. 62001.

Amirreza Aghakhani (S'16) received the B.S. degree in mechanical engineering from Sharif University, Tehran, Iran, in 2008. He is currently working toward the Ph.D. degree in mechanical engineering with Koc University, Istanbul, Turkey.

His current research interests include energy harvesting, piezoelectricity, impedance modeling, structural dynamics, and vibrations.

Mr. Aghakhani is a member of the American Society of Mechanical Engineers and the International Society for Optics and Photonics.

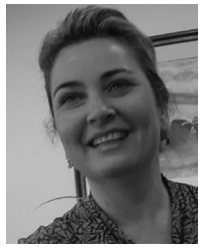

Ipek Basdogan received the Ph.D. degree in mechanical engineering from the University of Illinois at Chicago, Chicago, IL, USA, in 1997.

She is currently a Member of the Faculty with the Department of Mechanical Engineering, Koc University, Istanbul, Turkey. She is the Founder and Director of the Vibration and Acoustics Laboratory (VAL), Koc University. During her Ph.D., she worked at Argonne National Laboratory-Advanced Photon Source, Lemont, IL, USA. Before joining Koc University, she worked as a senior member of technical staff in the Guidance and Control Analysis Group, Jet Propulsion Laboratory, NASA, and Caltech, Pasadena, CA, USA between the years of 1997 and 2002. Her research interests include structural dynamics, active vibration control, design and optimization, energy harvesting, and vibro-acoustic analysis.